PAPER

Check for updates

Improved nanocomposite of montmorillonite and hydroxyapatite for defluoridation of water†

M. Shanika Fernando,[a] A. K. D. V. K. Wimalasiri,[a] S. P. Ratnayake,[b] J. M. A. R. B. Jayasinghe, [ID][a] Gareth R. William, [ID][c] D. P. Dissanayake,[a] K. M. Nalin de Silva [ID][a] and Rohini M. de Silva [ID]*[a]

A novel hydroxyapatite montmorillonite (HAP-MMT) nanocomposite system was synthesized using a simple wet chemical *in situ* precipitation method. Neat nano hydroxyapatite (HAP) was also synthesized for comparison. The characterization of the materials was carried out using Fourier Transform Infrared Spectroscopy (FT-IR), Scanning Electron Microscopy (SEM), X-ray diffraction (XRD) and Brunauer–Emmett–Teller (BET) isotherms to study the functional groups, morphology, crystallinity and the surface area respectively. Batch adsorption studies and kinetic studies on fluoride adsorption were conducted for the HAP-MMT system and for neat HAP. The effect of parameters such as contact time, pH, initial concentration, temperature, and thermodynamic parameters and the effect of coexisting ions on fluoride adsorption by HAP-MMT were studied. Results of the isotherm experiments were fitted to four adsorption isotherm models namely Langmuir, Freundlich, Temkin and Dubinin Radushkevich. Fluoride adsorption over HAP-MMT fitted to the Freundlich adsorption isotherm model and showed more than two-fold improved adsorption capacity (16.7 mg g^{-1}) compared to neat HAP. The best-fitting kinetic model for both adsorbents was found to be pseudo second order. Calculated thermodynamic parameters indicated that the fluoride adsorption by HAP-MMT is more favorable compared to that on HAP within the temperature range of 27 °C–60 °C. Improved fluoride adsorption by HAP-MMT is attributed to the exfoliated nature of HAP-MMT. Gravity filtration studies carried out using a 1.5 ppm fluoride solution, which is closer to the ground water fluoride concentrations of Chronic Kidney Disease of unknown etiology (CKDu) affected areas in Sri Lanka, resulted in a 1600 ml g^{-1} break through volume indicating the potential of HAP-MMT to be used in real applications.

1. Introduction

Fluoride is a naturally found element in water bodies and fluoride intake within the permissible levels is beneficial as an essential nutrient for the prevention of dental caries and making strong bones.[1] However, long-term consumption of water with fluorides at elevated levels (according to WHO above 1.5–2.0 ppm) can cause adverse health effects.[2] Dental and skeletal fluorosis is considered to be the most noticeable health hazard and is common in many parts of the world, including India and Sri Lanka.[3] In addition, it has also been identified that this can cause different types of chronic diseases that can affect renal, gastrointestinal and immunological systems.[4] Recently,

fluoride has been identified as one of the main causative agents for chronic kidney disease with unknown etiology (CKDu), in Sri Lanka, which is considered as one of the alarming health issues in the country.[5,6] Among the existing water defluorination methods, adsorption has been identified as one of the best methods and has been extensively studied and reviewed.[7–13] In comparison to the different types of bulk materials which have been studied for fluoride adsorption, metal oxides and hydroxides of titanium,[5,14] iron,[15,16] lanthanum[17] and aluminium[18] are identified as the most frequently studied materials with higher adsorption capacities. Further, different types of nanomaterials including other metal oxides[11,19–22] metal oxide hybrids[23,24] and hydroxides,[22,25–28] and carbon nanotubes,[29–31] have also been tested on removing fluoride ions. However, as indicated by Stanić *et al.*[32] these adsorbents have only a limited applicability due to their high cost and toxicity. Therefore, it is of utmost importance to find efficient and cost-effective alternative methods that can remove excessive levels of fluorides from water. Nano hydroxyapatite is a nontoxic material which has been extensively used in biomedical applications and HAP based nanocomposites have been identified as

[a]Centre for Advanced Materials and Devices (CAMD), Department of Chemistry, University of Colombo, Colombo 03, Sri Lanka. E-mail: rohini@chem.cmb.ac.lk

[b]Sri Lanka Institute of Nanotechnology (SLINTEC), Nanotechnology and Science Park, Pitipana, Homagama, Sri Lanka

[c]UCL School of Pharmacy, University College London, 29-39 Brunswick Square, London, WCIN 1AX, UK

promising materials in water purification.[30,33–35] Several researchers have studied the fluoride adsorption properties of nano hydroxyapatite which are synthesized by different methods and many of these resulted a comparatively low adsorption capacity with a long contact times.[36–39] In addition, the inherent affinity of cations such as Al towards fluoride has led many scientists to explore clay minerals as sorbents to water de-fluorination. In this regard, different type of clay minerals such as kaolinite,[40] montmorillonite,[41,42] bentonite,[43] pyrophyllite[44] and meixnerite[45,46] have been considered. Of these, clay minerals, montmorillonite (MMT) is a well-known smectite nano clay which is used in biomedical applications as well as to remove metal ions.[47,48] However, fluoride adsorption studies carried out with MMT has resulted very low fluoride adsorption capacities with long contact hours at neutral pH.[41] Therefore, in our study, incorporation of nano HAP with MMT nano clay was thought to improve adsorption properties of fluorides, as it may facilitate the creation of more adsorption sites to interact. Also the combination of nanohydroxyapatite and MMT was preferred as they are comparatively cheap materials which can be formed into a composite using a simple and cost effective one pot synthesis method, without maintaining high temperatures.

2. Materials and method

2.1. Materials

All the chemicals used were analytical grade and used without further purification. Ammonium hydroxide (NH_4OH solution, 25%, Sigma Aldrich), calcium nitrate tetrahydrate ($Ca(NO_3)_2 \cdot 4H_2O$, 98% Sigma Aldrich), di-ammonium hydrogen orthophosphate (($NH_4)_2HPO_4$, 98% Sigma Aldrich) were used to synthesis neat HAP. Montmorillonite (Sigma Aldrich) was used to synthesis HAP-MMT nanocomposites and sodium fluoride, 99.5% (Merck) was used to prepare the fluoride stock solutions.

2.2. Synthesis of hydroxyapatite nanoparticles

Nano hydroxyapatite was synthesized according to the modified method reported earlier by us.[7] In brief ($NH_4)_2HPO_4$ was added dropwise into $Ca(NO_3)_2 \cdot 4H_2O$ solution maintaining the Ca/P ratio to 1.67 at 60 °C with vigorous stirring. The pH was maintained at 10 with dropwise addition of NH_4OH (5 M) and then the mixture was vigorously stirred at its boiling point for about 3 h. The mixture was aged for 24 hours at room temperature and the HAP precipitate was washed until its pH became neutral. The product was separated by centrifugation. The resultant solid was oven dried at 80 °C until a constant weight was obtained.

2.3. Synthesis of HAP-MMT nanocomposites

5% (w/v) MMT was mixed with distilled water and kept overnight to swell and facilitate better exfoliation. Then the MMT slurry was stirred vigorously for 1 hour and *in situ* precipitation of HAP was carried out following the same procedure explained above. Samples where the HAP : MMT ratio of the final product to be 2 : 1, 1 : 1, 1 : 2 and 1 : 4 were synthesized in this manner.

The resulted product was washed and separated by centrifugation. Then it was oven dried at 80 °C for 3 hours. The nanocomposite prepared with HAP : MMT ratio 1 : 1 was identified as the best ratio as it gave the best defluorination capacity with a favourable texture (Refer S1 and S2 in the ESI†).

2.4. Characterization of the materials

Scanning Electron Microscopy (SEM) images of both HAP nanoparticles and HAP-MMT nanocomposite were obtained using a Hitachi SU6600 Scanning Electron Microscope (SEM) to analyses the surface characteristics of the adsorbents. Fourier Transform Infrared Spectrometer (FT-IR)-AVATAR-320 (Thermo Nicolet) was used to analyse the functional groups and the molecular interactions of the samples in the wave number range between 500 cm⁻¹ and 4000 cm⁻¹. Samples were prepared in the form of pellets using KBr, maintaining the KBr : sample mass ratio at 1 : 10. X-ray diffraction analysis of the synthesized HAP nanoparticles and HAP-MMT nanocomposite was performed using a Bruker D8 Focus X-ray powder diffractometer using CuKα radiation (= 0.154 nm) over the 2 θ range of 3°–60°, with a step size of 0.02° and a step time of 1 s. The Brunauer–Emmett–Teller (BET) surface area measurements were carried out using a Beckman coulter sorption analyser.

2.5. Fluoride adsorption studies

A stock solution of 100 ppm fluoride was prepared using sodium fluoride in a polypropylene container. Batch adsorption studies were carried out in polypropylene containers (60 ml) with constant agitation at 200 rpm with the aid of an orbital shaker.

The adsorption capacities were calculated according to eqn (1), where Q_e is the adsorption capacity (mg L⁻¹), C_0 is the initial concentration (mg L⁻¹), C_t is the concentration after contacting time (mg L⁻¹), V is the volume (L) of aqueous solution and m is the mass of the adsorbent (g).

$$Q_e = (C_0 - C_t)V/m \times 1000 \tag{1}$$

2.5.1. Analysis for fluorides. Fluoride concentrations of solutions were analysed using a fluoride ion selective electrode. Each sample (8.0 ml) was mixed with TISAB solution (8.0 ml) before measuring the electrode potential (mV) of the fluoride selective electrode (details are given in S2 in the ESI†).

2.5.2. Effect of time. The effect of time on the adsorption capacity was investigated at different time periods (1–240 min) for HAP and HAP-MMT, using 20.0 ml of 30 ppm fluoride solution and 0.02 g of adsorbent at room temperature (27 ± 1 °C) and at the pH of drinking water (6.5 ± 0.2).

2.5.3. Batch adsorption isotherm studies. Data for the adsorption isotherms were obtained in the concentration range of 1–30 ppm of fluoride for HAP-MMT and HAP with constant stirring at 200 rpm, for periods of 60 and 240 minutes, respectively.

Data obtained were analysed using four adsorption isotherm models (Langmuir, Freundlich, Temkin and Dubinin Radushkevich) in order to identify the best fitting isotherm model. The linearized form of the Langmuir adsorption isotherm that is used to describe monolayer adsorption is given in eqn (2).

$$C_e/Q_e = 1/Q_L k_L + C_e/Q_L \tag{2}$$

where, C_e, Q_e, K_L, Q_L are the concentration of the adsorbate at the equilibrium (mg L^{-1}), the adsorption capacity (mg g^{-1}), Langmuir isotherm constant (L mg^{-1}) and the maximum monolayer adsorption capacity (mg g^{-1}) respectively.

The linear forms of the Freundlich adsorption isotherm is illustrated in eqn (3) and the Freundlich adsorption isotherm is plotted against log Q_e *vs.* log C_e, where, Q_e and C_e are adsorption capacity (mg g^{-1}) and the concentration (mg L^{-1}) at the equilibrium while K_f, and n represent Freundlich adsorption isotherm constants.

$$\log Q_e = \log K_f + 1/n \log C_e \tag{3}$$

Temkin isotherm model which takes in to account the induced heterogeneity,[49] was also applied in linear form as given in the eqn (4), where q_e is the adsorption capacity, C_e is the concentration at the equilibrium, where, k_t is the Temkin isotherm binding constant, and B_t is the constant related to the heat of sorption.

$$q_e = B_t(\ln k_t) + B_t(\ln C_e) \tag{4}$$

The results of the adsorption data were also tested with the Dubinin–Radushkevich model which is given in the eqn (5), where q_e and Q_m are the adsorption capacity at the equilibrium and theoretical adsorption capacity in mg g^{-1} respectively. K_{DR} is the activity coefficient related to the free energy of adsorption and ε is known as Polanyi potential and ε_2 is calculated according to eqn (6).

$$\ln q_e = \ln(Q_m) - K_{DR}\varepsilon^2 \tag{5}$$

$$\varepsilon_2 = RT \ln(1+(1/C_e) \tag{6}$$

The mean of adsorption energy, E was calculated using the eqn 7.

$$E = 2K_{DR}^{1/2} \tag{7}$$

2.5.4. Kinetic studies. Kinetics for the defluorination by HAP and HAP-MMT was studied using a 30 ppm initial fluoride concentration. Results were fitted to pseudo first order, pseudo second order and intraparticle diffusion kinetic models. The linear form of the first order kinetics model can be expressed as in the general equation given in eqn (8) where q_e and q_t are the adsorption capacity (mg g^{-1}) at the equilibrium and time t and k_1 is the pseudo first order adsorption rate constant (min^{-1}).

$$\log(q_e - q_t) = \log(q_e) - k_1 t/2.303 \tag{8}$$

The pseudo second order kinetic model is given in the eqn (9), where k_2 is the pseudo second order rate constant.

$$t/q = 1/k_2 q_e^2 + 1/q_e t \tag{9}$$

Intraparticle diffusion model is described in the eqn (10), where q_t is the adsorption capacity (mg g^{-1}) k_p is the intraparticle diffusion rate constant (mg g^{-1} min$^{-1/2}$ g^{-1}) and C is the intercept,[50]

$$q_t = k_p t^{1/2} + C \tag{10}$$

2.5.5. The effect of pH on fluoride ion adsorption. In order to identify the improved adsorption properties of the HAP-MMT nanocomposite at the drinking water pH levels, the adsorption studies were carried out separately for HAP, MMT, HAP-MMT composites and also for a physical mixture of HAP, MMT with 1 : 1 ratio at different pH levels.[2–11] Experiments were conducted for 20 ml of 10 ppm fluoride solutions and the dose of the adsorbent at 0.04 g.

2.5.6. The effect of temperature and thermodynamic parameters. The adsorption studies were conducted at different temperatures (27 °C, 35 °C, 40 °C, 50 °C and 60 °C) for the removal of fluoride by both HAP and HAP-MMT separately by maintaining the identical reaction conditions such as initial fluoride concentration (15 ppm), adsorbent dosage (0.02 g), shaking time and the speed. Thermodynamic parameters, Gibbs free energy change ($\Delta G°$ kJ mol^{-1}), standard entropy change ($\Delta S°$ kJ^{-1} mol K^{-1}) and standard enthalpy change ($\Delta H°$ kJ mol^{-1}) were calculated by the following equations (eqn (11) and (12)) where R (J mol^{-1} K^{-1}) is the universal gas constant T is the temperature in kelvin. K_d is the distribution coefficient of the solute and K_d was calculated using C_a/C_e where C_a is the adsorbate concentration on the adsorbent at the equilibrium and C_e is the concentration of the adsorbate in the solution at the equilibrium.[51]

$$\Delta G° = RT \ln K_d \tag{11}$$

$$\ln K_d = \Delta S°/R - \Delta H°/RT \tag{12}$$

2.6. Effect of co-existing anions

In order to investigate the effect of co-existing ions on fluoride adsorption by both HAP and HAP-MMT adsorbents, separate adsorption studies were conducted using 10.0 ml of 10 ppm fluoride solutions. Study was conducted at two different concentrations (20 ppm and 200 ppm) of the ions namely, NO_3^-, NO_2^-, SO_4^{2-}, HCO_3^-, Cl^- and OH^-.

2.7. Gravity filtration

Gravity filtration studies were carried out using 1.5 ppm fluoride solution. The solution was passed at a rate of 0.33 ml s^{-1} through a column with a diameter of 1 cm across a filter bed prepared with HAP-MMT (0.05 g) deposited evenly on 0.05 g of

a cotton bed. The break through capacity was calculated using the volume of fluoride solution that could be passed through the column before the fluoride concentration of the filtrate exceeds 0.5 ppm.

2.8. Reusability test

Fluoride adsorbed HAP-MMT nanocomposite was used to test the reusability of the nanocomposite. Fluoride adsorbed HAP-MMT was filtered and separated from the solution and dipped in 1 M, NaOH overnight. Then it was washed well with double distilled water until the pH become neutral and oven dried. The samples were subjected for 3 cycles of fluoride adsorption.

3. Results and discussion

3.1. Characterization of the materials

Fig. S3 in ESI† illustrates the FTIR spectra of neat HAP, neat MMT and HAP-MMT respectively. The characteristic sharp peak at 3570 cm^{-1} (ref. 7) due to the OH stretching of HAP is clearly visible in the IR spectrum of HAP while neat MMT show a prominent peak at 3640 cm^{-1} due to OH stretching.[52] However, in HAP-MMT composite, there is a broad band in the region of 3700–3000 cm^{-1}. This can be attributed to the overlapping of the two peaks resulting from both neat HAP and MMT. The band at 1410 cm^{-1} in HAP-MMT composite can be credited to the duplex peak of HAP around 1400 cm^{-1} due to carbonate stretching. This indicates the successful incorporation of HAP in the composites. The presence of small peaks around 914–840 cm^{-1} region in both neat MMT and HAP-MMT composites and these peaks are due to Al and Mg ion interactions with OH– (Al$_2$OH near 920 cm^{-1}, Al–OH around 890 cm^{-1}, and OH– in Mg–OH near 840 cm^{-1}).[47–49] In addition, the band at 1035 cm^{-1} in neat HAP and HAP-MMT composites is due to phosphate stretching as reported in literature. This also confirms the successful incorporation of HAP into MMT.[53,54] The Scanning Electron Microscopy (SEM) images of MMT, HAP-MMT and fluoride adsorbed HAP-MMT (HAP-MMT-F) are shown in Fig. S4.† The SEM of neat HAP indicates that they are in the nanoscale similar to our previous work[7] with 80 nm of length and 30 nm of width and show a rod like morphology. The SEM image of neat MMT shows flat planes with continuous arrangement. In comparison, HAP-MMT composite shows expanded, disordered flakes with considerable number of pores with depositions of HAP and a large surface area. This exfoliated nature of HAP-MMT composite indicated that there is a higher tendency for exposing more cationic sites for F$^-$ to get bonded with. Higher surface area was further confirmed with BET data as discussed below. According to Fig. S4(d),† an extensive exfoliation of HAP-MMT composite can be seen after adsorption of F$^-$ ions. This image further revealed, peeled out plates like morphology of HAP-MMT composite indicating further expansion of the layers due to adsorption of F$^-$ ions at hydroxide sites of the intercalated space, as shown in the mechanism (Fig. 6). This is further supported by the XRD pattern observed for HAP-MMT composite (Fig. 1) which shows amorphous nature of MMT after F$^-$ being adsorbed.
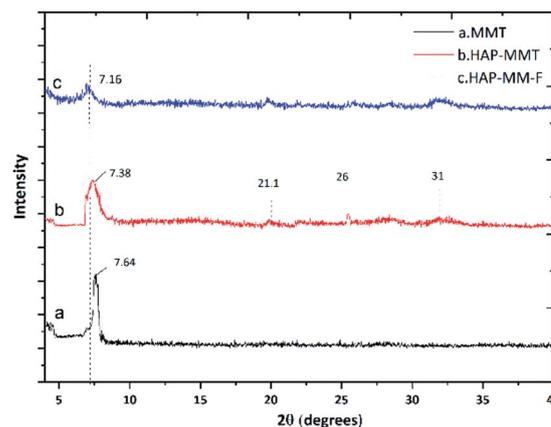

Fig. 1 XRD of MMT, HAP–MMT and fluoride adsorbed HAP–MMT (HAP–MMT–F).

As shown in Fig. 1, the X-ray diffraction pattern of neat MMT, HAP-MMT and HAP-MMT-F show prominent peaks at $2\theta = 7.64$, 7.38 and 7.16 respectively. In addition, two peaks corresponding to HAP at $2\theta = 21°$, 26° and 34° can also be seen with lower intensity in HAP-MMT composite and this indicates a successful synthesis of HAP.[55] The d-spacing which were calculated according to the Bragg's equation ($n\lambda = 2d \sin \theta$) corresponding to the prominent peaks resulted for MMT, HAP-MMT and HAP-MMT-F were 11.38 A°, 11.61 A° and 12.32 A° respectively. The enhancement of the d spacing in the formation of HAP-MMT indicated the intercalation of HAP nanoparticles in to the layers of MMT.[56] Expansion of layers to provide more spaces is also evident from BET isotherm analysis, where it was found to increase from 46.4 for neat HAP to 78.98 m^2 g^{-1} for HAP-MMT (resulted plots are given in Fig. S5 in the ESI†). Further enhancement of the d spacing in fluoride adsorbed HAP-MMT-F is in support of exfoliation of the structure in the process of fluoride adsorption.

3.2. Adsorption studies

3.2.1. Effect of contact time. The effect of contact time on the adsorption of F$^-$ ions for three composites were carried out using initial F$^-$ concentration of 30 ppm for 2 hours. The
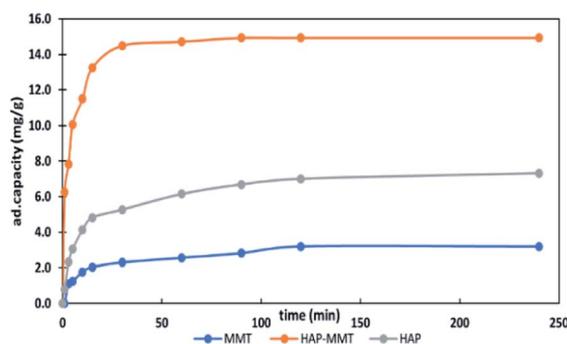

Fig. 2 Effect of contact time on the adsorption capacity of fluoride ions.
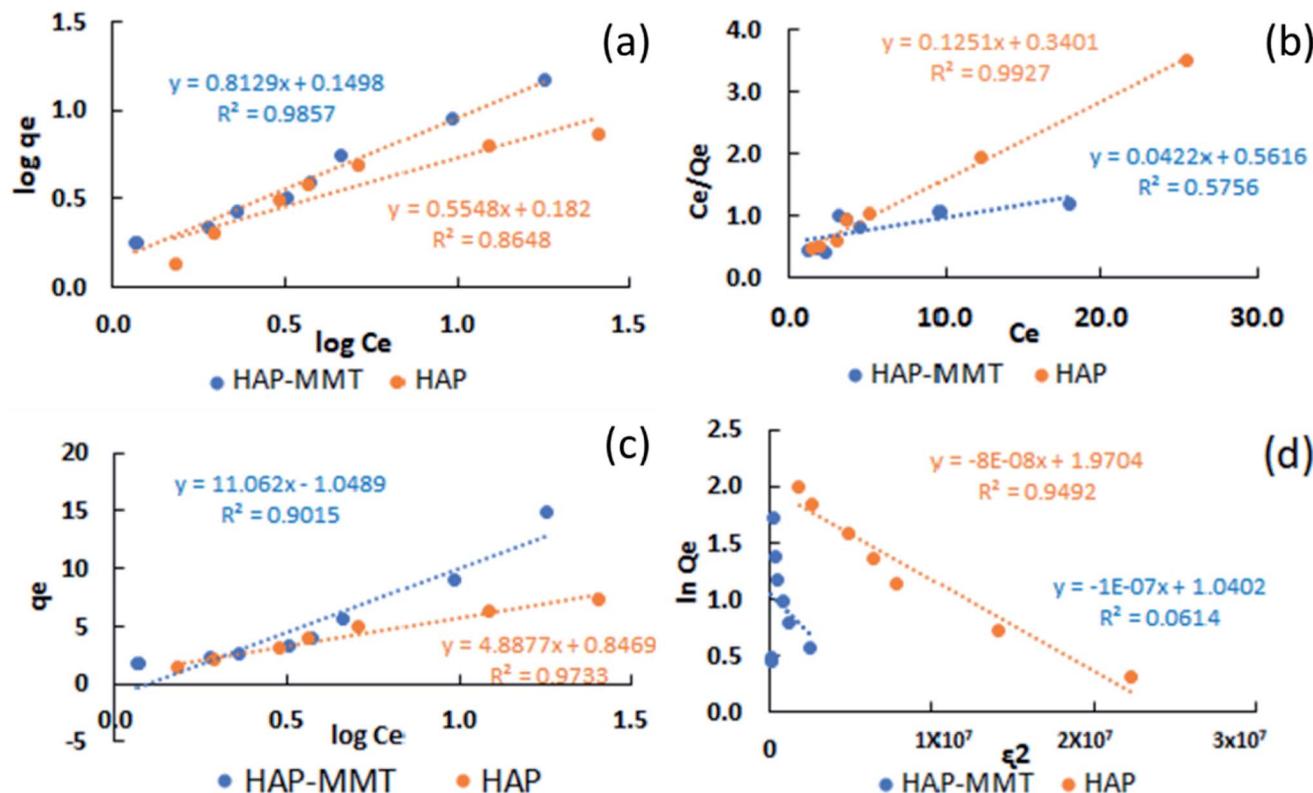
Fig. 3 (a) Langmuir, (b) Freundlich, (c) Temkin, (d) Dubinin Radushkevich adsorption isotherms for HAP–MMT and HAP.

graphical representation of the results is shown in Fig. 2. Accordingly, HAP-MMT shows the fastest kinetics and improved adsorption properties than that of neat HAP. Also, the results indicate that HAP-MMT reaches more than 50% of its maximum adsorption capacity within the first 5 minutes and reaches the maximum level within 30 minutes. Therefore, HAP-MMT was identified as the best system and only that system was subjected to batch adsorption studies and kinetic studies along with neat HAP for comparison.

3.3. Adsorption isotherms for fluorides

Adsorption isotherms are important to study the properties and the behaviour of the process of adsorption. Data obtained for the batch adsorption studies were fitted to four isotherm models (Freundlich, Langmuir, Temkin and Dubinin Radush-kevich) as explained in the experimental section.

Fig. 3 illustrates the resulted plots by all four isotherm models. Adsorption isotherm constants were calculated for each model and resulted values are summarized in Table 1 with

Table 1   Langmuir, Freundlich, Temkin and Dubinin Radushkevich isotherm constants for fluoride adsorption by neat HAP and HAP-MMT

		HAP-MMT	HAP
Experimental data	q_e (mg g^{-1})	14.90	7.32
Langmuir isotherm constants	Q_L (mg g^{-1})	23.70	6.71
	K_L (min^{-1})	14.15	3.43
	R^2	0.576	1.00
Freundlich isotherm constants	n	1.230	1.98
	Q_e (mg g^{-1})	16.71	6.98
	K_f (g mg^{-1} min^{-1})	1.41	1.60
	R^2	0.986	0.805
Temkin isotherm constants	K_t (L g^{-1})	0.910	1.327
	$B_t \times 10^3$	11.062	4.157
	R^2	0.902	0.904
Dubinin Rarushkevish isotherm constant	K_{DR} (mol^2 J^{-2})	1×10^{-7}	8×10^{-8}
	Q_m (mg g^{-1})	2.829	6.810
	E (kJ mol^{-1})	1.414	0.000
	R^2	0.061	0.961

Table 2 Kinetic constants for HAP-MMT and HAP on fluoride adsorption

		HAP-MMT	HAP
Experimental data	Q_e (exp) mg g^{-1}	14.92	7.32
Pseudo first order	k_1	−0.215	−0.208
	Q_e (cal) (mg g^{-1})	127.673	21.409
	R^2	0.8817	0.7922
Pseudo second order	Q_e (cal) mg g^{-1}	15.08	7.51
	k_2 (gmg^{-1}s)	0.014	0.020
	R^2	0.999	0.997
Intraparticle diffusion	K_p (mg g^{-1} min$^{-1/2}$)	2.5042	1.5546
	C	0.322	0.367
	R^2	0.7465	0.6560
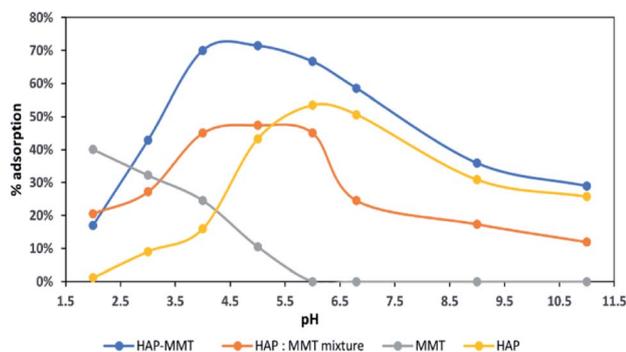
Fig. 4 The effect of pH on adsorption capacity of F$^-$ and adsorption percentage.

their correlation coefficients (R^2). Freundlich model was found to be the best model ($R^2 = 0.986$) that describes the fluoride adsorption by HAP-MMT. This indicates that the fluoride removal by HAP-MMT is characterized with a multilayer adsorption which is mostly shown by the systems with heterogenous surfaces.[30,35] The maximum adsorption capacity calculated for HAP-MMT, by the best fit Freundlich model was 16.7 mg g^{-1}, while the experimental adsorption capacity was found to be 14.9 mg g^{-1}. This value can be considered as a relatively high adsorption capacity when compared with the adsorption capacities obtained for other HAP based nanocomposites containing biocompatible materials.[52–54] Also, the n value calculated for HAP-MMT by the Freundlich model was 1.23 and this indicates that the process of adsorption is

favourable as the resulted value is below 10. The other models could be fitted in the order of Temkin ($R^2 = 0.902$), Langmuir ($R^2 = 0.576$) and D–R isotherm ($R^2 = 0.0614$). Temkin model can be used to describe a system with induced heterogeneity and D–R model is used to explain an adsorption mechanism of Gaussian energy distribution on a heterogeneous surface. In comparison fluoride adsorption on neat HAP was fitted well with the Langmuir adsorption isotherm ($R^2 = 0.993$) and resulted a 6.71 mg g^{-1}.

3.4. Adsorption kinetics

In addition to the adsorption isotherms, kinetic data were obtained for both neat HAP and HAP-MMT at 30 ppm initial concentration of fluoride to evaluate the kinetic model and the kinetic constantans. Kinetic data were fitted in to pseudo-first-order, pseudo-second-order and intraparticle diffusion models and the resulted plots are shown in the Fig. S6 in ESI.† The kinetic constants of the three models (k_1, k_2, k_p), the adsorption capacity calculated by the kinetic models and the experimentally resulted adsorption capacities (Q_e (cal.) and Q_e (exp.)) and the correlation coefficients (R^2) are calculated and tabulated in Table 2. Maximum monolayer adsorption capacity while the other isotherm models were fitted in the order of D–R ($R^2 = 0.9614$), Temkin ($R^2 = 0.904$) and Freundlich ($R^2 = 0.805$).

According to the results, pseudo second order kinetic model show comparatively higher R^2 values for both HAP-MMT and HAP. In addition, the kinetics data show that the values of q_e, $q_{(cal.)}$ by pseudo second order kinetic model are closer to the experimental q_e value at both the concentrations (Table 2). Therefore, it can be predicted that the adsorption of fluorides on both nano HAP and HAP-MMT follow pseudo second order kinetic model.

3.5. Effect of pH

The effect of pH is considered as one of the important parameters that can affect the process of adsorption, as changing pH can alter the surface charges of the adsorbents. The effect of pH was tested from pH 2–11 for neat HAP, neat MMT, HAP-MMT nanocomposite and also for the mixture of neat HAP and neat MMT in the same ratio as in the HAP-MMT composite by keeping all the other parameters constant. According to the results illustrated in Fig. 4, HAP-MMT nanocomposite shows the highest adsorption percentage of 71% at pH 5. However, externally mixed HAP/MMT which was prepared by mixing HAP

Table 3 Thermodynamic parameters of fluoride adsorption for HAP and HAP-MMT

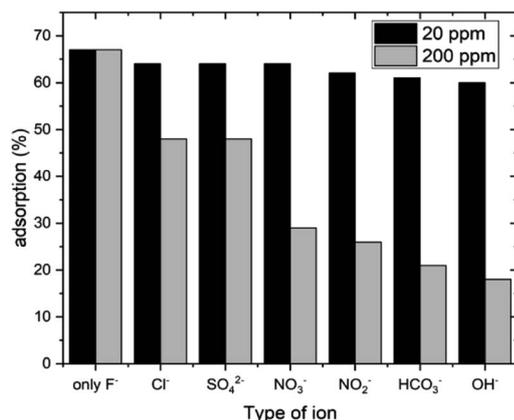| Temp (K)	HAP-MMT			HAP		
	$\Delta G°$ (kJ mol^{-1})	$\Delta S°$ (kJ mol^{-1} K^{-1})	$\Delta H°$ (kJ mol^{-1})	$\Delta G°$ (kJ mol^{-1})	$\Delta S°$ (kJ mol^{-1} K^{-1})	$\Delta H°$ (kJ mol^{-1})
300	−0.92	0.16	47.42	0.85	0.20	61.85
308	−2.02			0.18		
313	−3.31			−1.31		
323	−3.94			−2.58		
333	−4.72			−3.04		

Fig. 5 Fluoride adsorption capacity in the presence of other ions for 60 minutes.

and MMT in to the same ratio of HAP-MMT showed a lower adsorption capacity.

This indeed indicated the need of exfoliated MMT structure with more adsorption sites for the adsorption of fluoride ions. MMT shows very poor fluoride adsorption and the highest adsorption capacity (40%) was observed at pH 2 where no adsorption could be observed at pH of normal drinking water or higher. Also, neat HAP showed a lower adsorption capacity compared to HAP-MMT at all the tested pH values. From these studies it is clear that only HAP-MMT system is suitable for drinking water purification.

3.6. The effect of temperature and thermodynamics

Thermodynamic parameters of an adsorption process can be used to determine its feasibility. Results obtained for the adsorption studies at different temperatures show that the adsorption capacities of both HAP and HAP-MMT are increased

when the temperature is increased from 27 °C–60 °C indicating the endothermic nature of the process of adsorption. The results were used to calculate the thermodynamic parameters and the values obtained for ΔG°, ΔS° and ΔH° are tabulated in Table 3. The graph of $\ln K_{d}$ vs. $1/T$ which was used for the calculations of thermodynamic parameters for HAP-MMT and fluoride is given in Fig. S6 in ESI.† According to the ΔG° values, fluoride adsorption by HAP-MMT is characteristic with a more favourable adsorption of fluoride. Positive ΔH° value indicates that the adsorption process is endothermic. These observations agree with literature, as similar results have been reported for different adsorbents under varying experimental conditions.[39,55,56]

3.7. Effect of other ions

The uptake of fluoride can be affected by other common ions present in water as they can act as competitive ions in the process of fluoride adsorption. Therefore, the adsorption of fluoride ions by HAP-MMT was investigated using other ions (NO_3^{-}, NO_2^{-}, SO_4^{2-}, HCO_3^{-}, Cl^{-} and OH^{-}) that may present in ground water. Two ion concentrations (20 ppm and 200 ppm) were used to investigate this. Results of the experiment are given in Fig. 5. It can be seen that there is a significant reduction in fluoride adsorption when the interfering ions are present at high concentrations. The highest interference was observed for OH^{-} ions at both the tested concentrations. Interfering strength of the ions is in the order $OH^{-} > HCO_3^{-} > NO_2^{-} > NO_3^{-} > SO_4^{2-} > Cl^{-}$.

3.8. Reusability

In order to test the reusability of HAP-MMT, a sample of HAP-MMT was subjected to repeated fluoride adsorption. The material was regenerated as explained in the experimental section, prior to be used for fluoride adsorption. It was observed that the adsorption capacity was slightly decreased after each
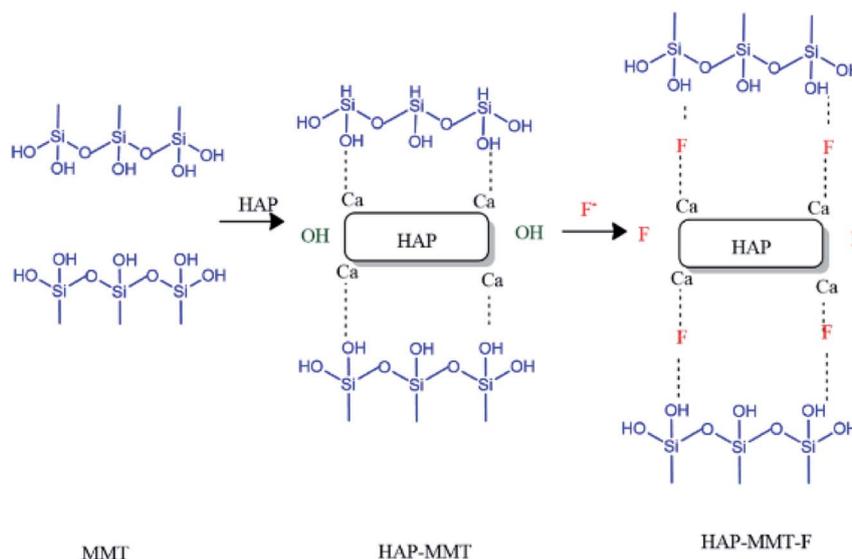

Fig. 6 Suggested mechanism explaining improved fluoride adsorption by HAP–MMT composite.
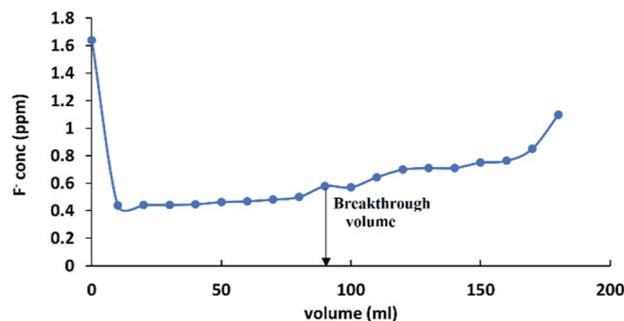
Fig. 7 Breakthrough curve for fluoride adsorption on to HAP-MMT.

regeneration cycle as the resulted percentage of fluoride adsorption changed from, 55%, 43% and 37% in three consecutive regeneration cycles. This shows that a complete desorption of fluorides ions has not taken place during regeneration.

3.9. Mechanism of adsorption

Fluoride adsorption by HAP has been proposed to occur *via* two pathways, namely by ion exchange with lattice OH⁻ and by interaction with cationic centres.[39,55,56] In the present work, we have observed an improved fluoride adsorption when HAP is interacting with MMT. In addition to the increment in surface area, the arrangement of adsorption sites may have played a role in improving the fluoride adsorption capacity. The very low uptake of fluoride by MMT at pH 5.5–7.0 range and the significant improvement of fluoride uptake by HAP-MMT composite support this argument. The synergistic effect on fluoride adsorption is clearly evident as the *in situ* synthesized HAP-MMT material has a significantly high fluoride adsorption capacity compared to the physical mixture of HAP and MMT having the same molar ratio. Based on the structural data, morphological analysis and surface

area measurements, mechanism involved in the adsorption of F⁻ ions onto HAP-MMT composite could be suggested to follow the mechanism in Fig. 6. Accordingly, the possible initial step could be the immobilization of Ca^{2+} ions within the layers of MMT by anchoring onto hydroxyl groups. This may attract the phosphate ions resulting the formation of HAP on both internal and external surfaces. This can be attributed to the expansion of MMT layer as observed in XRD data (Fig. 1) and SEM data (Fig. S3(c)†). Due to this expansion, more OH⁻ groups may now be available for F⁻ ions to exchange with. In addition, the involvement of Ca^{2+} in anchoring F⁻ with MMT may also play a role in improving the fluoride adsorption capacity.

3.10. Breakthrough capacity calculated by gravity filtration

Gravity filtration studies were carried out to identify the feasibility of using HAP-MMT nanocomposite in field applications. According to a recent study, the average fluoride concentration of the CKDu affected areas in Sri Lanka has been identified to be in the range of 1.5–0.5 ppm[59–62] while non CKDu areas were reported with fluoride concentration below 0.5 ppm. In addition, dental fluorosis has also been reported with low concentration ranges and many studies indicate 0.5 ppm of fluoride as the desirable level in drinking water. Therefore, in this work, gravity filtration studies were conducted using 1.5 ppm of fluoride solution as the initial concentration and 0.5 ppm was considered as the safe limit, for fluorides. The break through capacity was calculated using the volume that could reduce the concentration of 1.5 ppm fluoride solution up to 0.5 ppm, when it is passed through a column with 1 cm diameter at a flow rate of 0.33 ml s⁻¹. The breakthrough curve is represented in Fig. 7 and the break through volume for 0.05 g was found as 80 ml as show in the graph. Therefore, it can be calculated as 1600 ml g⁻¹ for a unit mass. According to the literature, many adsorbents are not capable of adsorbing fluoride at concentrations below 2 ppm in the pH range of drinking water pH (5.5–7).[32]

Table 4 Comparison of fluoride adsorption properties of HAP-MMT nanocomposite with other reported HAP based materials

| Adsorbent (mm) | Concentration range or highest concentration used (ppm) | Contact Time (min) | Adsorption capacity (mg g⁻¹) | Filter bed column studies | | | | |
				Initial concentration	Flow rate	Diameter, thickness of column	Break through capacity	Ref.
Modified HAP with activated alumina	10–200	480	14.4	3	Not given	11	400 L g⁻¹	63
Al-HAP	200	180	98.8	5	10 ml min⁻¹	2, 0.3	1568 L m⁻²	64
HAP-MMT	30	30	16.7	1.5	10 ml min⁻¹	10, 0.2	1600 L g⁻¹	This work
HAP-alginate	10	30	3.87	Not reported				57
HAP-cellulose	10	360	4.2	Not reported				35
Magnetic HAP-alginate	10	30	4.05	Not reported				15
HAP-CTS	10	30	1.56	Not reported				65
Multiwall CNT-HAP	3–50	150	30.22	Not reported				30
HAP-gelatin	8–14		4.157	Not reported				58
CNT-HAP	—	300	11.05	Not reported				58
Mineral substituted HAP	10	60	8.36	Not reported				66

In addition, Table 4 was used to compare the adsorption properties resulted from batch adsorption studies and gravity filtration studies of some of the reported HAP based nanocomposites prepared using nontoxic bulk materials such as biopolymers. According to that the HAP-MMT nanocomposite of this work show a considerably good adsorption capacity and a short contact time. To the best of our knowledge, gravity filtration studies reported in literature have been conducted considering 1.5 ppm as the safe limit. However, in the present study, we have demonstrated that the HAP-MMT nanocomposite can be used to lower the fluoride concentration down to 0.5 ppm.

4. Conclusion

A novel material for fluoride adsorption has been synthesized by incorporating hydroxyapatite (HAP) in to montmorillonite (MMT). The resultant material has a high fluoride adsorption capacity in the pH range of drinking water compared to a physical mixture of HAP and MMT. The improvement in fluoride adsorption is suggested to be the expansion of layers of MMT and incorporation of HAP in to the layers. The fluoride adsorption capacities of MMT, HAP and HAP-MMT were 2.44, 6.7 and 16.7 mg g^{-1} respectively. Also, the gravity filtration studies indicated that the HAP-MMT is a promising material which can be applied in real applications.

Conflicts of interest

There are no conflicts of interest to declare.

Acknowledgements

References

1 D. Kanduti, P. Sterbenk and B. Artnik, Fluoride: A Review of Use and Effects on Health, *Mater. Soc. Med.*, 2016, **28**(2), 133, available from: http://www.scopemed.org/fulltextpdf.php?mno=223171.

2 World Health Organization, *Guidelines for Drinking-water Quality Fourth Edition WHO Library Cataloguing, in Publication Data Guidelines for drinking-water quality*, 4th edn, 2017, available from: http://www.who.int.

3 S. L. Choubisa, L. Choubisa and D. K. Choubisa, Endemic Fluorosis in Rajasthan, *Indian J. Environ. Health*, 2001, **43**(4), 177–189.

4 D. Browne, H. Whelton and D. O'Mullane, Fluoride metabolism and fluorosis, *J. Dent.*, 2005, **33**(3), 177–186.

5 K. Babaeivelni and A. P. Khodadoust, Adsorption of fluoride onto crystalline titanium dioxide: Effect of pH, ionic strength, and co-existing ions, *J. Colloid Interface Sci.*, 2013, **394**(1), 419–427, DOI: 10.1016/j.jcis.2012.11.063.

6 R. W. Dharmaratne, Fluoride in drinking water and diet: the causative factor of chronic kidney diseases in the North Central Province of Sri Lanka, *Environ. Health Prev. Med.*, 2015, **20**(4), 237–242.

7 M. Shanika Fernando, R. M. De Silva and K. M. Nalin De Silva, Synthesis, characterization, and application of nano hydroxyapatite and nanocomposite of hydroxyapatite with granular activated carbon for the removal of Pb^{2+} from aqueous solutions, *Appl. Surf. Sci.*, 2015, **351**, 95–103.

8 H. Aissam, F. Errachidi, M. J. Penninckx, M. Merzouki and M. Benlemlih, Production of tannase by Aspergillus niger HA37 growing on tannic acid and Olive Mill Waste Waters, *J. Microbiol. Biotechnol.*, 2005, 609–614.

9 D. Zhang, H. Luo, L. Zheng, K. Wang, H. Li, Y. Wang, *et al*. Utilization of waste phosphogypsum to prepare hydroxyapatite nanoparticles and its application towards removal of fluoride from aqueous solution, *J. Hazard. Mater.*, 2012, **241–242**, 418–426, available from: https://www.sciencedirect.com/science/article/pii/S0304389412009995.

10 A. Teimouri, S. Ghanavati Nasab, S. Habibollahi, M. Fazel-Najafabadi and A. N. Chermahini, Synthesis and characterization of a chitosan/montmorillonite/ZrO$_2$ nanocomposite and its application as an adsorbent for removal of fluoride, *RSC Adv.*, 2015, **5**(9), 6771–6781, DOI: 10.1039/C4RA13139H.

11 Short Communication Pyrolysis of Coconut Shell and its Potential as Fuel, *Agric. Wastes*. 1986, **17**, 313–317.

12 M. Yesilbas, M. Holmboe and J. F. Boily, Cohesive vibrational and structural depiction of intercalated water in montmorillonite, *ACS Earth Space Chem.*, 2018, **2**(1), 38–47.

13 L. Wang, Y. Xie, J. Yang, X. Zhu and Q. Hu, RSC Advances Insight into mechanisms of fluoride removal from contaminated groundwater using lanthanum- modified bone waste, *RSC Adv.*, 2017, 54291–54305.

14 Z. Zhou, Y. Yu, Z. Ding, M. Zuo and C. Jing, Competitive adsorption of arsenic and fluoride on {201} TiO$_2$, *Appl. Surf. Sci.*, 2019, **466**, 425–432.

15 Y. Zhang, X. Lin, Q. Zhou and X. Luo, Fluoride adsorption from aqueous solution by magnetic core-shell Fe$_3$O$_4$@alginate-La particles fabricated *via* electro-coextrusion, *J. Hazard. Mater.*, 2016, **389**, 34–45, DOI: 10.1016/j.apsusc.2016.07.087.

16 Y. Huang, Y. Shih and C. Chang, Adsorption of fluoride by waste iron oxide: the effects of solution pH, major coexisting anions , and adsorbent calcination temperature, *J. Hazard. Mater.*, 2011, **186**(2–3), 1355–1359, DOI: 10.1016/j.jhazmat.2010.12.025.

17 P. Mondal and S. George, A review on adsorbents used for defluoridation of drinking water, *Rev. Environ. Sci. Biotechnol.*, 2015, **14**(2), 195–210.

18 Y. H. Li, S. Wang, A. Cao, D. Zhao, X. Zhang, C. Xu, *et al.* Adsorption of fluoride from water by amorphous alumina supported on carbon nanotubes, *Chem. Phys. Lett.*, 2001, **350**(5–6), 412–416.

19 A. Ghosh, S. Chakrabarti, K. Biswas and U. C. Ghosh, Agglomerated nanoparticles of hydrous Ce(IV) + Zr(IV) mixed oxide: Preparation, characterization and physicochemical aspects on fluoride adsorption, *J. Hazard. Mater.*, 2014, **307**, 665–676, DOI: 10.1016/j.apsusc.2014.04.095.

20 S. P. Suriyaraj and R. Selvakumar, Advances in nanomaterial based approaches for enhanced fluoride and nitrate removal from contaminated water, *RSC Adv.*, 2016, **6**(13), 10565–10583, DOI: 10.1039/C5RA24789F.

21 C. Xu, J. Li, F. He, Y. Cui, C. Huang, H. Jin, *et al.* Al_2O_3-Fe_3O_4-expanded graphite nano-sandwich structure for fluoride removal from aqueous solution, *RSC Adv.*, 2016, **6**(99), 97376–97384.

22 V. A. Online, L. Chen, J. He, X. Cai and J. Liu, Performance and mechanism of hierarchically porous Ce-Zr oxide 2 nanospheres encapsulated calcium alginate beads for fluoride removal from water, *RSC Adv.*, 2016.

23 S. Raghav and D. Kumar, Adsorption Equilibrium, Kinetics, and Thermodynamic Studies of Fluoride Adsorbed by Tetrametallic Oxide Adsorbent, *J. Chem. Eng. Data*, 2018, **63**(5), 1682–1697, DOI: 10.1021/acs.jced.8b00024.

24 C. Zhang, Y. Li, T. Wang, Y. Jiang and H. Wang, Applied Surface Science Adsorption of drinking water fluoride on a micron-sized magnetic Fe_3O_4 @ Fe-Ti composite adsorbent, *J. Hazard. Mater.*, 2016, **363**, 507–515, DOI: 10.1016/j.apsusc.2015.12.071.

25 J. Wang, W. Xu, L. Chen, Y. Jia, L. Wang, X. Huang, *et al.* Excellent fluoride removal performance by CeO_2 – ZrO_2 nanocages in water environment, *Chem. Eng. J.*, 2013, **231**, 198–205.

26 S. Deng, H. Liu, W. Zhou, J. Huang and G. Yu, Mn – Ce oxide as a high-capacity adsorbent for fluoride removal from water, *J. Hazard. Mater.*, 2011, **186**(2–3), 1360–1366, DOI: 10.1016/j.jhazmat.2010.12.024.

27 L. Chen, B. He, S. He, T. Wang, C. Su and Y. Jin, Fe–Ti oxide nano-adsorbent synthesized by co-precipitation for fluoride removal from drinking water and its adsorption mechanism, *Powder Technol.*, 2012, **227**, 3–8, DOI: 10.1016/j.powtec.2011.11.030.

28 T. Wu, L. Mao and H. Wang, Adsorption of fluoride on Mg/Fe layered double hydroxides material prepared *via* hydrothermal process, *RSC Adv.*, 2015, **5**(30), 23246–23254, DOI: 10.1039/C4RA16839A.

29 C. Binns, *Introduction to Nanoscience and Nanotechnology*, 2010.

30 Z. Y. Ruan, Y. X. Tian, J. F. Ruan, G. J. Cui, K. W. Iqbal, A. Iqbal, *et al.* Synthesis of hydroxyapatite/multi-walled carbon nanotubes for the removal of fluoride ions from solution, *J. Hazard. Mater.*, 2017, **412**, 578–590, DOI: 10.1016/j.apsusc.2017.03.215.

31 Q. Tang, T. Duan, P. Li, P. Zhang and D. Wu, Enhanced Defluoridation Capacity From Aqueous Media *via* Hydroxyapatite Decorated With Carbon Nanotube, *Front. Chem.*, 2018, **6**.

32 M. Habuda-Stanić, M. Ravančić and A. Flanagan, A Review on Adsorption of Fluoride from Aqueous Solution, *Materials*, 2014, **7**(9), 6317–6366, available from: http://www.mdpi.com/1996-1944/7/9/6317/.

33 D. C. Manatunga, R. M. de Silva, K. M. N. de Silva and R. Ratnaweera, Natural polysaccharides leading to super adsorbent hydroxyapatite nanoparticles for the removal of heavy metals and dyes from aqueous solutions, *RSC Adv.*, 2016, **6**(107), 105618–105630.

34 H. Zhang, X. Shi, A. Tian, L. Wang and C. Liu, Electrochemical properties of Ti^{3+} doped Ag-Ti nanotube arrays coated with hydroxyapatite, *J. Hazard. Mater.*, 2018, **436**, 579–584, DOI: 10.1016/j.apsusc.2017.12.048.

35 X. Yu, S. Tong, M. Ge and J. Zuo, Removal of fluoride from drinking water by cellulose@hydroxyapatite nanocomposites, *Carbohydr. Polym.*, 2013, **92**(1), 269–275, DOI: 10.1016/j.carbpol.2012.09.045.

36 V. Sternitzke, R. Kaegi, J.-N. Audinot, E. Lewin, J. G. Hering and C. A. Johnson, Uptake of Fluoride from Aqueous Solution on Nano-Sized Hydroxyapatite: Examination of a Fluoridated Surface Layer, *Environ. Sci. Technol.*, 2012 Jan 17, **46**(2), 802–809, DOI: 10.1021/es202750t.

37 G. E. J. Poinern, M. K. Ghosh, Y. J. Ng, T. B. Issa, S. Anand and P. Singh, Defluoridation behavior of nanostructured hydroxyapatite synthesized through an ultrasonic and microwave combined technique, *J. Hazard. Mater.*, 2011, **185**(1), 29–37.

38 V. Sternitzke and C. A. Johnson, Adsorption of fluoride on synthetic hydroxyapatite, *Geochim. Cosmochim. Acta*, 2009, **73**(13), A1273.

39 S. Gao, J. Cui and Z. Wei, Study on the fluoride adsorption of various apatite materials in aqueous solution, *J. Fluorine Chem.*, 2009, **130**, 1035–1041.

40 B. Bar Yosef, I. Afik and R. Rosenberg, Fluoride sorption by montmorillonite and kaolinite, *Soil Sci.*, 1988, **145**(3), 195–200.

41 G. Karthikeyan and A. Pius GA, Fluoride adsorption studies of montmorillonite clay, *Indian J. Chem. Technol.*, 2005, **12**, 263–272.

42 A. Tor, Removal of fluoride from an aqueous solution by using montmorillonite, *Desalination*, 2006, **201**(1–3), 267–276, available from: https://www.sciencedirect.com/science/article/pii/S0011916406011714.

43 S. P. Kamble, P. Dixit, S. S. Rayalu and N. K. Labhsetwar, Defluoridation of drinking water using chemically modified bentonite clay, *Desalination*, 2009, **249**(2), 687–693.

44 J. H. Kim, C. G. Lee, J. A. Park, J. K. Kang, N. C. Choi and S. B. Kim, Use of pyrophyllite clay for fluoride removal from aqueous solution, *Desalin. Water Treat.*, 2013, **51**(16–18), 3408–3416.

45 Q. Guo and E. J. Reardon, Fluoride removal from water by meixnerite and its calcination product, *Appl. Clay Sci.*, 2012, **56**, 7–15, DOI: 10.1016/j.clay.2011.11.013.

46 A. Vinati, B. Mahanty and S. K. Behera, Clay and clay minerals for fluoride removal from water: A state-of-the-art

review, *Appl. Clay Sci.*, 2015, **114**, 340–348, DOI: 10.1016/j.clay.2015.06.013.

47 D. Qin, X. Niu, M. Qiao, G. Liu, H. Li and Z. Meng, Adsorption of ferrous ions onto montmorillonites, *J. Hazard. Mater.*, 2015, **333**, 170–177, DOI: 10.1016/j.apsusc.2015.02.019.

48 Campinas-unicamp UE De, C. D. R. Minerais and Matogrosso-ufmt UF De. Performance of modified montmorillonite clay in mercury adsorption process and thermodynamic studies. 2008, **11**, 20–23.

49 V. Bolis, C. Morterra, B. Fubini, P. Ugliengo and E. Garrone, Temkin-Type Model for the Description of Induced Heterogeneity: CO Adsorption on Group 4 Transition Metal Dioxides, *Langmuir*, 1993, **9**(6), 1521–1528.

50 O. Rahmanian, M. Dinari and M. K. Abdolmaleki, Carbon quantum dots/layered double hydroxide hybrid for fast and efficient decontamination of Cd(II): The adsorption kinetics and isotherms, *J. Hazard. Mater.*, 2018, **428**, 272–279, DOI: 10.1016/j.apsusc.2017.09.152.

51 P. Saha and S. Chowdhury, *Thermodynamics*, ed. M. Tadashi, InTech, 2011, pp. 350–360.

52 F. Lin, G. Zhu, Y. Shen, Z. Zhang and B. Dong, Study on the modified montmorillonite for adsorbing formaldehyde, *J. Hazard. Mater.*, 2015, **356**, 150–156, DOI: 10.1016/j.apsusc.2015.07.186.

53 M. B. Ahmad, K. Shameli, W. Zin and W. Yunus, Synthesis and Characterization of Silver/Clay/Starch Bionanocomposites by Green Method, *Adv. Mater.*, 2010, **4**(7), 2158–2165.

54 G. M. Poralan, J. E. Gambe, E. M. Alcantara and R. M. Vequizo, X-ray diffraction and infrared spectroscopy analyses on the crystallinity of engineered biological hydroxyapatite for medical application, *IOP Conf. Ser.: Mater. Sci. Eng.*, 2015, **79**(1).

55 B. Nayak, A. Samant, R. Patel and P. K. Misra, Comprehensive Understanding of the Kinetics and Mechanism of Fluoride Removal over a Potent Nanocrystalline Hydroxyapatite Surface, *ACS Omega*, 2017, 8118–8128.

56 N. Madusanka, K. M. N. De Silva and G. Amaratunga, Curcumine activated carboxymethyl cellulose-montmorillonite clay nanocomposite having enhanced curcumine release in aqueous media, *Carbohydr. Polym.*, 2015, **134**, 695–699, DOI: 10.1016/j.carbpol.2015.08.030.

57 K. Pandi and N. Viswanathan, Synthesis of alginate bioencapsulated nano-hydroxyapatite composite for selective fluoride sorption, *Carbohydr. Polym.*, 2014, **112**, 662–667, DOI: 10.1016/j.carbpol.2014.06.029.

58 K. Pandi and N. Viswanathan, In situ precipitation of nano-hydroxyapatite in gelatin polymatrix towards specific fluoride sorption, *Int. J. Biol. Macromol.*, 2015, **74**, 351–359, DOI: 10.1016/j.ijbiomac.2014.12.004.

59 R. Chandrajith, J. P. Padmasiri, C. B. Dissanayake and K. M. Prematilaka, Spatial distribution of fluoride in groundwater of Sri Lanka, *J. Natl. Sci. Found. Sri Lanka*, 2012, **40**(4), 303–309.

60 K. E. Levine, J. H. Redmon, M. F. Elledge, K. P. Wanigasuriya, K. Smith, B. Munoz, *et al.* Quest to identify geochemical risk factors associated with chronic kidney disease of unknown etiology (CKDu) in an endemic region of Sri Lanka— a multimedia laboratory analysis of biological, food, and environmental samples, *Environ. Monit. Assess.*, 2016, **188**(10), 548, DOI: 10.1007/s10661-016-5524-8.

61 C. B. Dissanayake and R. Chandrajith, Groundwater fluoride as a geochemical marker in the etiology of chronic kidney disease of unknown origin in Sri Lanka, *Ceylon J. Sci., Biol. Sci.*, 2017, **46**(2), 3, DOI: 10.4038/cjs.v46i2.7425/.

62 S. Wickramarathna, S. Balasooriya, S. Diyabalanage and R. Chandrajith, Tracing environmental aetiological factors of chronic kidney diseases in the dry zone of Sri Lanka–A hydrogeochemical and isotope approach, *J. Trace Elem. Med. Biol.*, 2017, **44**, 298–306, DOI: 10.1016/j.jtemb.2017.08.013.

63 G. Tomar, A. Thareja and S. Sarkar, Enhanced fluoride removal by hydroxyapatite-modified activated alumina, *Int. J. Environ. Sci. Technol.*, 2015, **12**(9), 2809–2818, DOI: 10.1007/s13762-014-0653-5.

64 J. He, K. Chen, X. Cai, Y. Li, C. Wang, K. Zhang, *et al.* A biocompatible and novelly-defined Al-HAP adsorption membrane for highly effective removal of fluoride from drinking water, *J. Colloid Interface Sci.*, 2017, **490**, 97–107, DOI: 10.1016/j.jcis.2016.11.009.

65 C. Sairam Sundaram, N. Viswanathan and S. Meenakshi, Uptake of fluoride by nano-hydroxyapatite/chitosan, a bioinorganic composite, *Bioresour. Technol.*, 2008, **99**(17), 8226–8230.

66 A. Nagaraj, M. A. Munusamy, M. Ahmed, S. Suresh Kumar and M. Rajan, Hydrothermal synthesis of a mineral-substituted hydroxyapatite nanocomposite material for fluoride removal from drinking water, *New J. Chem.*, 2018, **42**(15), 12711–12721.